Rheology, birefringence, and small-angle neutron scattering in a charged micellar system: Evidence of a shear-induced phase transition

E. Cappelaere,[1] J. F. Berret,[2] J. P. Decruppe,[1] R. Cressely,[1,*] and P. Lindner[3]
[1]*Laboratoire de Physique des Liquides et des Interfaces, Groupe Rhéophysique des Colloïdes, Université de Metz, 1 Boulevard F. Arago, 57070 Metz, France*
[2]*Groupe de Dynamique des Phases Condensées, UMR CNRS No. 5581, Université de Montpellier II, F-34095 Montpellier Cedex 05, France*
[3]*Institut Laue-Langevin, Boîte Postale 156, F-38042 Grenoble Cedex 9, France*
(Received 21 January 1997)

We report here the experimental results on the first-order isotropic to nematic phase transition induced by shear in a concentrated micellar solution of cetyltrimethylammanium bromide (CTAB) without salt. We use and compare the results obtained under shear on the same solution with the help of four different techniques: rheology (stress and shear rate controlled), flow birefringence (FB), and small-angle neutron scattering under shear (SANSUS). The system without salt studied here is a model system. The rheological data show that the shear stress σ, as a function of the shear rate, allows one to distinguish three domains: a Newtonian regime (I) for $\dot{\gamma} < \dot{\gamma}_{1c}$, where the viscosity remains constant and equal to η_0 (zero shear viscosity); a plateau of the shear stress, noted II for $\dot{\gamma}_{1c} < \dot{\gamma} < \dot{\gamma}_{2c}$; and a third domain (III) corresponding to the turnup of the shear stress for $\dot{\gamma} > \dot{\gamma}_{2c}$. For the shear rate belonging to domain II, FB shows two different concentric layers of liquid presenting different anisotropic properties. SANSUS measurements in domains II and III indicate that the structure factor of the strongly oriented phase is identical to that of a nematic phase. This complete study of the salt-free CTAB system allows one to describe the phase transition induced by shear and to show that there is good agreement with the results obtained with the four techniques. [S1063-651X(97)06707-X]

PACS number(s): 05.70.Fh

I. INTRODUCTION

Surfactant solutions are aqueous solutions of molecules having hydrophobic and hydrophilic parts and are known to exhibit fascinating properties. These surfactant molecules in solutions are known to self-assemble above the critical micellar concentration to form micelles. The size and flexibility of rodlike and wormlike micelles are mainly imposed by surfactant volume fraction, salt concentration, and temperature. The properties of the wormlike micellar solutions have been found to be parallel to those of flexible polymers up to a certain point [1–4]. However, these micellar systems are found to be different from classical polymer solutions: the micellar chains are equilibrium objects and they can reversibly break and recombine.

The dynamic behavior of complex fluids such as surfactant solutions in the nonlinear regime has been the subject of intensive research in recent years. The rheological response results for sufficiently large values of the shear rate $\dot{\gamma}$ from nonequilibrium systems. From a mechanical point of view, the nonlinear response of a material is governed by its constitutive equation. For steady shear, a constitutive scheme was proposed by Cates [5] for entangled wormlike micellar systems that exhibit Maxwellian behavior. This equation was solved by Spenley, Cates, and McLeish [6]. The fundamental result is that in steady shear, the shear stress saturates to a constant value giving rise to a stress plateau. On the other hand, it is shown that the morphology of micelles and even their respective phases that are formed in surfactant solutions can be modified by shear [7].

The rheology of the unscreened micellar systems (polyelectrolytes) is not well understood. In the absence of salt, the electrostatic interactions modify significantly the rheological properties [8–10]. The variation of the viscosity of semidilute micellar solutions with surfactant volume fraction was found to be larger than that of the neutral system [11]. This was interpreted as being due to an abrupt increase of micellar size resulting from electrostatic interactions. The theory of the growth of the micelles in systems without salt described by Mackintosh, Safran, and Pincus [12] concerns volume fraction $\phi \ll 1$. In our experimental study, ϕ is not far from the value giving a liquid-crystalline phase and pretransitional effects cannot be neglected. The system studied in this work shows all the rheological characteristics of concentrated systems. Electrostatic interactions between cetyltrimethylammanium bromide (CTAB) molecules add to the sterical constraints and this has an important influence on the length of the micelles.

Most of the experimental and theoretical works on wormlike micelles were performed on screened micelles. The wormlike screened micelles are well characterized [11,13–17]. It has been shown recently that the shearing of an isotropic (I) solution of wormlike micelles can induce a first-order phase transition towards a nematic (N) phase [18]. Early experimental evidence of the shear-induced I-N transition was due to neutron scattering under shear for solutions of $CPClO_3$-$NaClO_3$ [19] and of CPCl-hexanol-brine [18]. A

*Address for correspondence: Université de Metz, Institut de Physique, LPLI, Groupe Rhéophysique des Colloïdes, 1 Boulevard Arago, 57078 Metz Cedex 3, France. FAX: 03-87-31-58-01. Electronic address: Cressely@lpli.univ-metz.fr

nematic phase induced by shear has been confirmed up to now by the following experimental observations: (i) near the nematic phase, strong orientational correlations are evidenced, (ii) the critical shear rate $\dot{\gamma}_{1c}$ and the ratio σ_c/G_0 values decrease and tend to zero as one approaches the phase boundary (G_0 is the elastic modulus), and (iii) beyond the transition shear rate $\dot{\gamma}_{1c}$, crescentlike scattering patterns obtained by small-angle neutron scattering (SANS), characteristic of orientational nematic order, show up in the direction perpendicular to the flow.

In a previous work [8], we have studied the CTAB-H_2O system in the concentrated region. We found a plateau behaviour $\sigma=\sigma_c$ of the shear stress and two different layers of liquid presenting different anisotropic properties in flow birefringence experiments. In this study, the highly birefringent layer was assumed to be a nematic phase. Here we extend our preceding experimental study on the CTAB system using two more techniques: the shear rate controlled rheology to test the robustness of the shear stress plateau and the small-angle neutron scattering to study the order parameter of the induced phase. A quantitative analysis of the results of SANS and flow birefringence (FB) leads to the determination of the proportion of the isotropic and nematic phase over the entire domain of shearing, i.e., from 0.1 to 6000 s^{-1}.

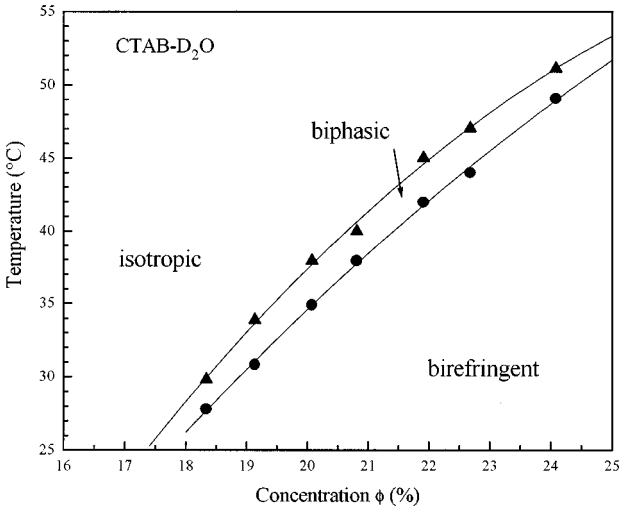

FIG. 1. Static phase diagram of the CTAB-D_2O system shown in terms of temperature versus surfactant concentration ϕ. With increasing ϕ, three regions are identified: isotropic, biphasic (isotropic and birefringent), and birefringent. For the latter, close to the phase boundary (open circles), the birefringent solution is nematic, as evidenced by their rheological and structural properties. At higher concentration, translational order also occurs (hexagonal).

II. EXPERIMENT

A. Products

Our study was carried out on aqueous salt-free solutions of CTAB. The CTAB (surfactant) product is commercially available (Janssen Chimica and Aldrich-Chemie). Here we focus on a unique solution CTAB-D_2O at $\phi=18\%$. The use of deuterated water was dictated by the SANS experiments in order to increase the scattering contrast between aggregates and surrounding solvent.

B. Phase diagram

The phase diagram of CTAB-D_2O solutions is displayed in Fig. 1. It was derived using birefringence measurements. It strongly resembles the (T, ϕ) phase diagram of CTAB-H_2O that we have recently reported [8]. For a given temperature, in Fig. 1 this phase diagram exhibits the isotropic-nematic phases sequence with increasing ϕ. We can note also the existence of a biphasic region, which is absent from the CTAB-H_2O situation. All the following experiments were performed at the same concentration $\phi=18\%$ (and usually at $T=32\,^{\circ}C$ for the comparison of the results obtained by the three techniques). Under these conditions, this sample is isotropic at rest and is considered as representative of the evolution of the phenomenon reported in this work.

C. Rheology

The linear and nonlinear viscoelastic properties of the CTAB solutions were obtained, on the one hand, on a Carrimed CSI 100 working in the *constant shear stress mode* and using a cone plane device (4 cm, 0.5°), which leads to a wide range of shear rate (the shear rate could be varied from 1 to 6000 s^{-1} approximately). On the other hand, a Rheometrics Fluid Spectrometer (RFS II) working in the *constant shear rate mode* and Couette configuration (a gap of 1 mm and a mean radius of 16.5 mm) was used. With the later system, steady shear measurements were checked to be in the stationary state of shearing up to 1750 s^{-1}. For the controlled stress rheometry, the magnitude of the complex viscosity $\eta^*(\omega)$, the storage modulus $G'(\omega)$, and the loss moduls $G''(\omega)$ were measured in an angular frequency range between $\omega=1$ and 250 rad s^{-1} at 32 °C. For the controlled strain rheometry, dynamical measurements were carried out for angular frequency $\omega=0.5-50$ rad s^{-1} at the same temperature (32 °C).

The fresh surfactant solutions as well as the solutions that were submitted to shearing stress or shearing strain during an experiment were completely transparent and free from foam and air bubbles. For each experiment we used a new sample.

D. Flow birefringence

The solution is studied in a conventional Couette cell with co-axial cylinders. The inner cylinder is the rotating one. The cell is built mainly from stainless steel, with a few parts in glass and Teflon; its dimensions are a height of 3 cm and radii of 4.7 and 5 cm for the inner and outer cylinders, respectively. The cell is placed between crossed polarizers. Under shear, two quantities of interest have to be determined: the angle of extinction χ, which defines the orientation of the medium, and the retardation φ (or the birefringence Δn) induced by the flow. χ is the acute angle formed by the streamline and a neutral line of the medium and is readily measured by rotating the polarizer-analyzer pair, which remains crossed, until the extinction is realized again: in that case the direction of polarization will be the same as the direction of a neutral line of the flowing medium. A quarter wave plate is added to measure the retardation φ according to the method of Senarmont. The birefringence

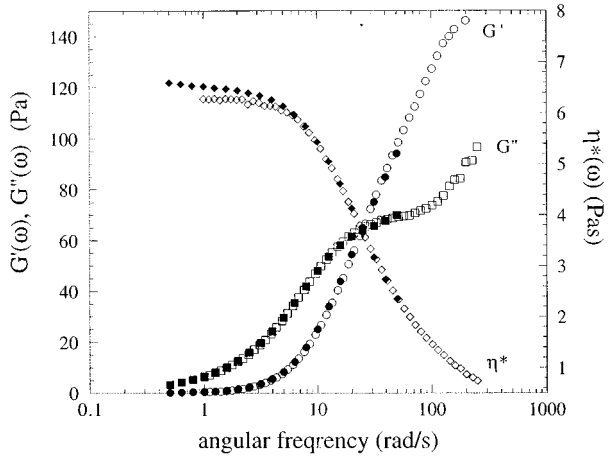

FIG. 2. Variation of the storage modulus $G'(\omega)$, the loss modulus $G''(\omega)$, and the dynamical viscosity $\eta^*(\omega)$ as a function of the angular frequency ω for the CTAB-D_2O solution at surfactant concentration $\phi=18\%$ ($T=32$ °C). Closed and open symbols have been obtained using strain and stress controlled rheometers, respectively.

intensity Δn is readily evaluated from the relation $\Delta n = \varphi\lambda/2\pi e$, where e is the thickness of the sample and is equal to the height of the Couette cell (wavelength $\lambda = 6328$ Å). χ and Δn are measured as a function of the shear rate at 32 °C. We have only added a source of white light to illuminate the entire gap when we photograph the flow [20].

E. Small-angle neutron scattering under shear

The small-angle neutron scattering measurements were carried out on the instrument D11 at the high flux reactor of the Institut Laue-Langevin (Grenoble). A 1-mm-gap Couette cell designed for SANS experiments [21] was utilized as shearing device in the range $0.1-2000\ s^{-1}$. The incoming neutron beam encounters the sample in a direction normal to the axis of rotation of the Couette cell, crossing twice the sheared solutions. The incident wave vector is thus parallel to the velocity gradient and perpendicular with respect to the flow velocity and vorticity. For isotropic and liquid-crystalline solutions studied in this work, the Couette-to-detector distance was chosen to be 2.5 m and the neutron wavelength 6 Å. This corresponds to momentum transfers varying from 1.6×10^{-2} to 1.3×10^{-1} Å^{-1}. Data are collected on a two-dimensional (2D) detector (64×64 elements of 1×1 cm^2) and displayed alternatively as 2D isointensity contours or 3D plots. A typical measuring time for one spectrum was 3 min.

III. RESULTS

A. Linear rheology

A detailed account of the linear rheology of salt-free CTAB-H_2O rodlike micelles has already been provided in an earlier report [8]. Figure 2 represents the dependence of G', G'', and η^* with the pulsation ω for CTAB-D_2O at $\phi=18\%$. The measurements were obtained from stress controlled (open symbols) and strain controlled (closed symbols) rheometry. The agreement between both measurements, as evidenced in Fig. 2, attests to the reliability of the rheometers

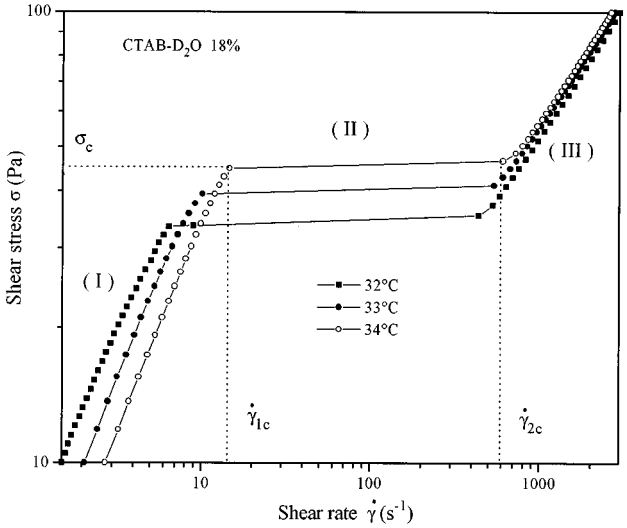

FIG. 3. Shear stress variation of the shear rate as measured for the CTAB-D_2O solution at $\phi=18\%$ using stress controlled rheometry ($T=32$ °C, 33 °C, and 34 °C). The flow curves exhibit a true discontinuity at a characteristic shear rate $\dot\gamma_{1c}$. In the intermediate range, no data points can be collected with the controlled stress rheometry. At rates about $\dot\gamma\approx440\ s^{-1}$, the stress increases again.

used in this study. Both experimental systems provided a static viscosity $\eta_0=6.7\pm0.3$ Pa s. Note that the real and imaginary parts of the complex modulus cross at $\omega\approx25$ rad/s and $G'=G''\approx65$ Pa. Above this crossover, $G'(\omega)$ continues to increase, indicating shorter relaxation times. The behavior is not of a Maxwellian type, but there is instead a disperse spectrum of relaxation time, as one would expect for a polydisperse system of unbreakable chains. We observe a striking analogy with entangled polymer solutions.

B. Nonlinear rheology

In Fig. 3 we display the shear stress as a function of the shear rate for the CTAB-D_2O at $\phi=18\%$, as measured from stress controlled rheometry. Data have been obtained in the stationary limit of flow at three different temperatures: $T=32$ °C, 33 °C, and 34 °C. From Fig. 3 three domains of evolution of the flow curves can be distinguished. The first corresponds to the Newtonian regime, where the stress varies linearly with the shear rate. As the shear stress is increased, the shear rate jumps from the lower to the higher branch of the flow curve. Clearly, in Fig. 3 no data points are obtained in the plateau region from controlled stress measurements. The plateau value $\sigma=\sigma_c$ begins for $\dot\gamma=\dot\gamma_{1c}$ and finishes for $\dot\gamma=\dot\gamma_{2c}$. We can see in the figure that the plateau value σ_c is strongly dependent on and increases with the temperature. For $\dot\gamma>\dot\gamma_{2c}$ we can observe here another increase of the shear stress. In the third domain, all the flow curves are practically superimposed. With the rheometer working in the constant shear stress mode, we can see in Fig. 4 that with our equilibrium measurements there is no experimental point between $\dot\gamma_{1c}$ and $\dot\gamma_{2c}$ giving the same $\sigma=\sigma_c$. With the rheometer in the constant shear rate mode, there are experimental points between $\dot\gamma_{1c}$ and $\dot\gamma_{2c}$. It is a fundamental difference between the two rheological modes of investigation. In Fig. 4 we show the nonlinear viscoelastic response received from

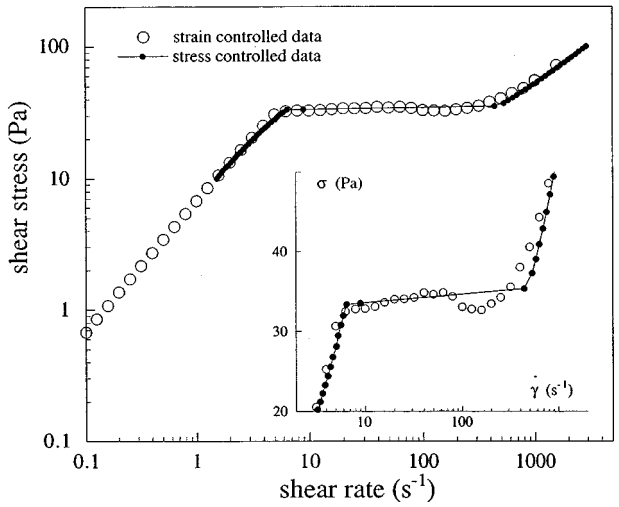

FIG. 4. Comparison between the $\sigma(\dot{\gamma})$ values in a log-log representation obtained with a controlled shear rate (open symbols) and a controlled shear stress (closed symbols) rheometer for the CTAB-D_2O without salt system at $T=32$ °C. Shown in the inset is the variation of the shear stress versus shear rate in a semilogarithmic representation.

strain controlled rheometry ($T=32$ °C). As mentioned above, in a log-log representation, we find again three distinctive ranges in strain rates. Below $\dot{\gamma}_{1c}\approx 6.5$ s^{-1}, the Newtonian regime is again in agreement with a static viscosity $\eta_0=6.7$ Pa s. Beyond this characteristic rate, the stress levels off and remains constant at 32 Pa. It is of the utmost importance to recall that each data point in the plateau region has been obtained in the stationary limit. Actually, in the plateau region, $\sigma(t)$ transient relaxations are present and these relaxations can last up to several minutes [8]. Around $\dot{\gamma}\approx 400$ s^{-1}, the shear stress increases again (regime III). Also included in Fig. 4 are the data from stress controlled rheometry. The agreement is again excellent. Both approaches evidence the three shear regions I, II, and III, but, in addition, the shear rates associated with the onsets of the plateau and of the upturn coincide quite well. In order to emphasize this agreement, we have plotted in the inset, in lin-log scales, the same data. This inset indicates that the stress plateau in a concentrated wormlike micellar solution is robust and independent of the working mode (stress or strain controlled).

C. Flow birefringence experiments

1. Qualitative observation of the flow birefringence

The results of our visual observations of the entire gap are represented by a set of five photographs taken at a temperature of 32 °C (Fig. 5). We can distinctly see two different concentric layers of liquid presenting different anisotropic properties. A bright thin line taking the shape of the inner cylinder appears in the gap when $\dot{\gamma}$ reaches a value ($\dot{\gamma}\approx 6.5$ s^{-1}) called $\dot{\gamma}_{1c}$ [Fig. 5(a)]. The two different bands correspond to the phenomenon of a shear banding structure appearing when the shear rate becomes greater than a critical value. In these situations we obtain a flowing separated biphasic structure: the bright zone corresponds to a strongly oriented phase and the dark zone corresponds to the isotropic phase. The isotropic phase is used here in opposition to the liquid crystal for the bright zone. As we shall see by quantitative flow birefringence measurements in domains I and II, we can measure the evolution of its birefringence with $\dot{\gamma}$; so, strictly speaking, this zone is also anisotropic. Measurements of the birefringence with our flowing device is not possible in the bright zone. We can note on Figs. 5(b)–5(d) that the width of the bright zone increases with $\dot{\gamma}$ to become a bright wide band [Fig. 5(e)] extending practically over the annular gap for $\dot{\gamma}\approx 400$ s^{-1} (shear rate belonging to the beginning of domain III for the temperature $T=32$ °C).

2. Measurements of χ and Δn

Quantitative measurements are presented in Fig. 6. This figure show the curves of the birefringence intensity Δn and extinction angle χ as functions of the shear rate for the 18% solution in deuterated solvent. A sharp crossover is found in the $\chi(\dot{\gamma})$ curves and corresponds roughly to the emergence of the bright zone mentioned before; the value of the shear rate that corresponds to this break is therefore the critical shear rate $\dot{\gamma}_{1c}$ introduced in the flow curves (see Fig. 4). As we can see in the same figure, the $\Delta n(\dot{\gamma})$ curve shows a linear increase of Δn with small shear rates up to a critical value of $\dot{\gamma}$ where also a break appears. The slope of the curve $\Delta n(\dot{\gamma})$ should gradually decrease towards zero and Δn should reach a smoothly saturation value, which indicates that despite the increase of $\dot{\gamma}$, the degree of orientation does not increase anymore. We can finally notice that the critical shear rates for $\chi(\dot{\gamma})$ and $\Delta n(\dot{\gamma})$ (corresponding to a break in the curves) are approximately the same.

D. Small-angle neutron scattering under shear flow

Figures 7 and 8 display the three-dimensional plots of the neutron intensities as received on the detector (raw data) for the $\phi=18\%$ CTAB-D_2O solution. Four representative values of the shear rates have been selected: 4, 102, 250, and 1403 s^{-1}, respectively. In order to allow comparisons with earlier works [22,23], we also show in Figs. 8(a)–8(d) the isointensity contours related to the same four patterns. The arrows on the 3D plots indicate the direction in real space of the flow velocity. In the following, this axis in reciprocal space will be refered to as $\mathbf{Q}_v$, while the orthogonal direction will be noted $\mathbf{Q}_e$ (e defines the vorticity). The set of vectors ($\mathbf{Q}_v$, $\mathbf{Q}_e$) actually determines the two coordinate axes in the contour representation used in Fig. 8. We emphasize that the full scales are in both directions ± 0.133 Å^{-1}.

At rest as well as at low shear rates (<10 s^{-1}), the pattern consists of an isotropic ring, as illustrated in Figs. 9(a) and 10(a). The structure factor exhibits a huge maximum at $Q_{\max}=0.074$ Å^{-1} as a function of the wave vector. This peak in the structure factor is usually assigned to strong correlations of the center of masses of the surfactant aggregates. Similar results have been obtained by many authors on low-concentration solutions of electrostatically charged particles [12,22–24] or on concentrated solutions of sterically interacting micelles [18]. The inverse $Q_{\max}$ value ($2\pi/Q_{\max}$) for the present CTAB system gives ~ 80 Å. As the strain rate is increased above ~ 10 s^{-1}, patterns become anisotropic. The anisotropy is characterized by two crescentlike peaks in the $\mathbf{Q}_e$ direction, indicating some ordering (alignment) process

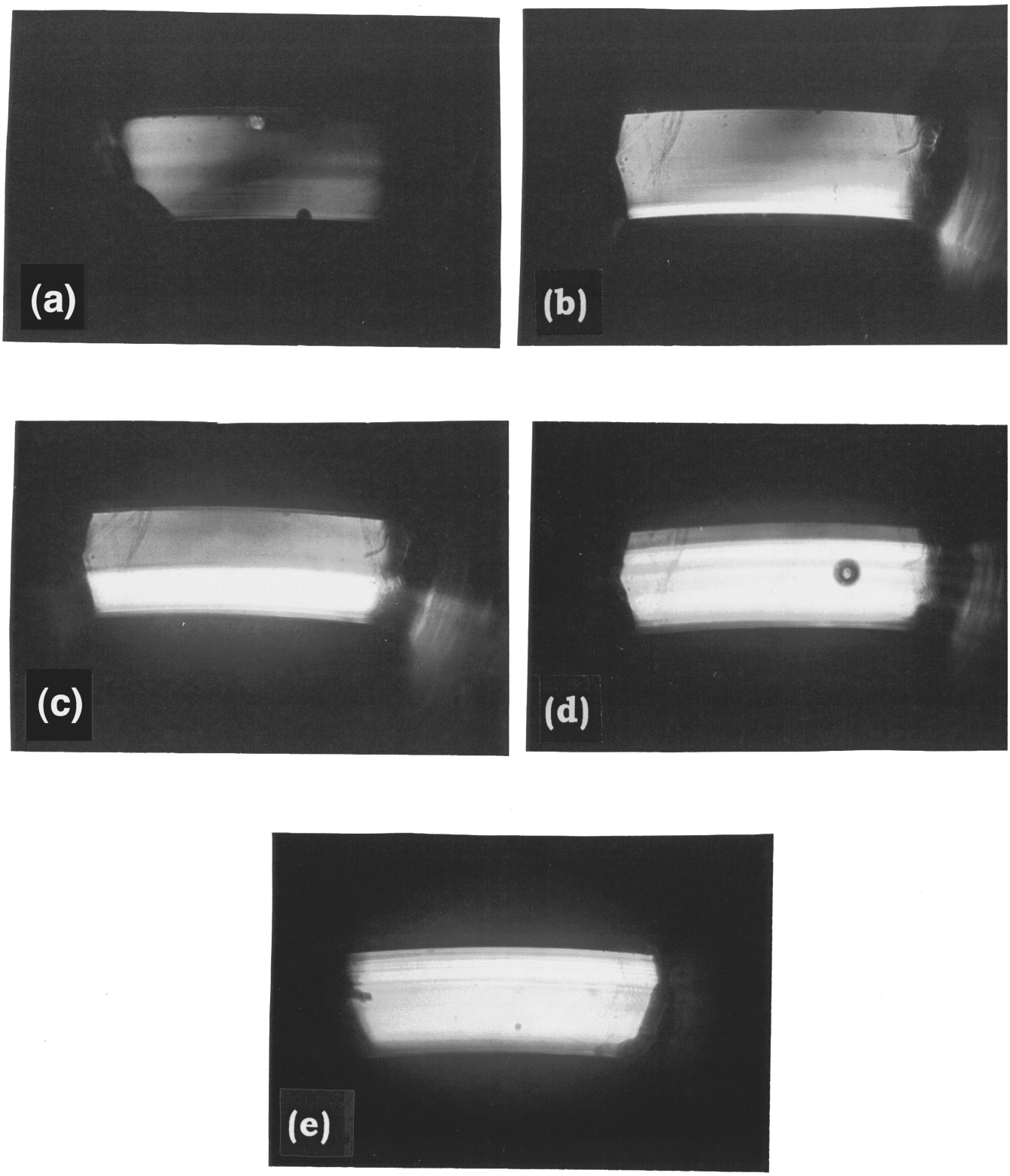

FIG. 5. Photographs of the 1.5-mm gap of a Couette shearing cell containing a CTAB-D_2O solution at $\phi = 18\%$. The five photographs correspond to the different domains (I–III) of the curves flow (see Fig. 4): (a) domain I, (b)–(d) domain II, and (e) domain III.

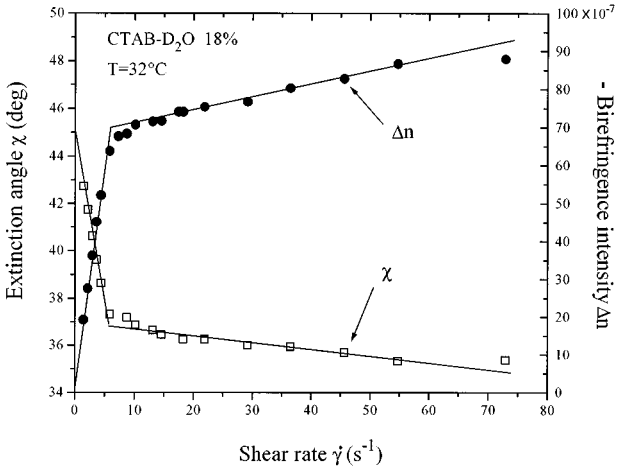

FIG. 6. Variation of the birefringence intensity Δn and the extinction angle χ vs the shear rate for the CTAB-D_2O system at $\phi = 18\%$ ($T = 32\,^{\circ}C$). The critical shear rates corresponding to the break of the $\chi(\dot{\gamma})$ and $\Delta n(\dot{\gamma})$ curves are approximately the same and correspond to $\dot{\gamma}_{1c}$.

of the aggregates induced by the shear. The crescentlike intensities grow progressively with $\dot{\gamma}$, whereas the isotropic ring vanishes. This is particularly obvious in the qualitative comparison of the patterns at $\dot{\gamma} = 102$ and $250\ s^{-1}$ [Figs. 7(b) and 7(c)]. At still higher shear rate ($1403\ s^{-1}$), the entire scattered intensity is contained in the anisotropic peaks located at $Q_e = \pm 0.074\ \text{Å}^{-1}$.

Finally, the neutron patterns arising from the sheared isotropic micellar solutions at $\phi = 18\%$ are compared with the one obtained on a liquid-crystalline CTAB-D_2O nematic sample at a slightly higher concentration and subjected to a modest shearing. Shown in Figs. 7(e) and 8(e) are the 3D plot and the map of contours of isointensity for a $\phi = 20\%$ CTAB-D_2O solution, which is nematic at rest, and for $\dot{\gamma} = 21.5\ s^{-1}$. The qualitative resemblance between this structure factor and the one obtained at high shear rates for the $\phi = 18\%$ sample [Fig. 7(d)] is rather impressive. We shall use this qualitative agreement to argue that this latter solution has undergone under shear a first-order phase transition towards a nematic oriented state (as when we increase the concentration at rest).

IV. ANALYSIS AND DISCUSSION

In this paper we have combined four different techniques to track the state of stationary shear flow of a salt-free micellar solution of CTAB: stress and shear rate controlled rheology, flow birefringence, and small-angle neutron scattering under shear. Some of these techniques have been used already and reported recently for parallel aims, but on different surfactant systems, such as CPCl-hexanol-brine [18], $CPClO_3$-$NaClO_3$ [19], CTAB-H_2O [8,21], and CPCl-salicylate-brine [14,15], and by different research groups. Here a different isotropic salt-free solution of cylindrical aggregates of surfactant is thoroughly investigated under shear using the four experimental methods mentioned above. This approach provides us with the opportunity to show unambiguously that simple shear applied to such concentrated micellar solution is able to trigger a nonequilibrium phase transition. The initial state is isotropic (at rest and low shear rates) and the final phase (high shear rates) is nematic, i.e., characterized by long-range orientational order (nonzero nematic order parameter).

In order to discuss and analyze the major findings of this work, we start with the shear rheology. As far as the mechanical response is concerned, a common behavior for the

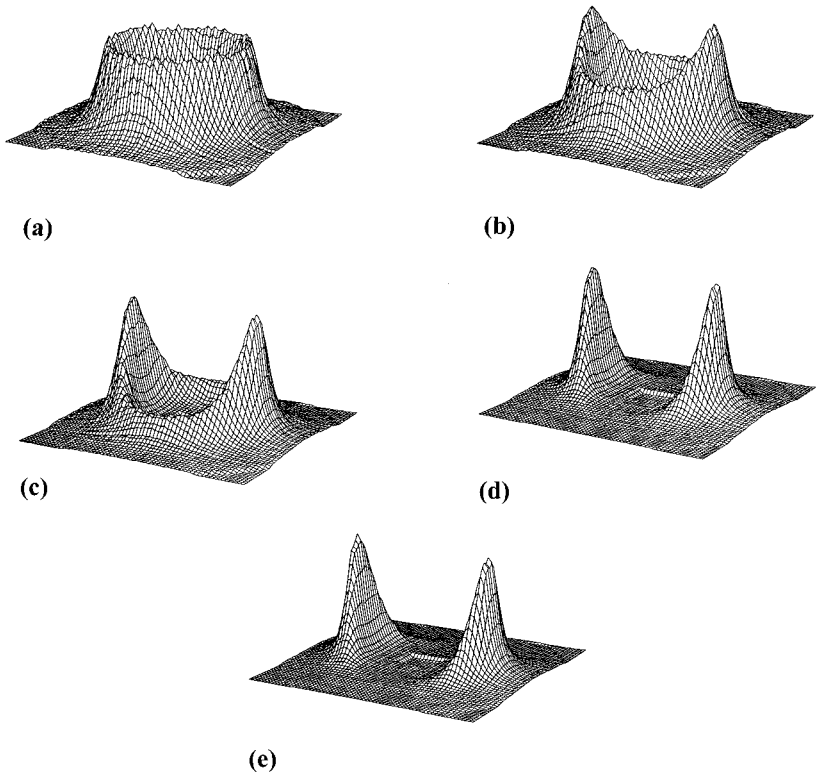

FIG. 7. Isometric intensity plots of the CTAB-D_2O system as observed on the two-dimensional detector. (a)–(d) Plots of measurements made at four different shear rates at 32 °C: (a) domain I ($\dot{\gamma} = 4\ s^{-1}$), (b) and (c) domain II ($\dot{\gamma} = 102$ and $250\ s^{-1}$, respectively), and (d) domain III ($\dot{\gamma} = 1403\ s^{-1}$). (e) CTAB-$D_2O$ nematic solution at $\phi = 20\%$ sheared at low $\dot{\gamma} = 21.5\ s^{-1}$ and at the same temperature. The full scale in both the $\mathbf{Q}_v$ and $\mathbf{Q}_e$ directions is ± 0.133 Å.

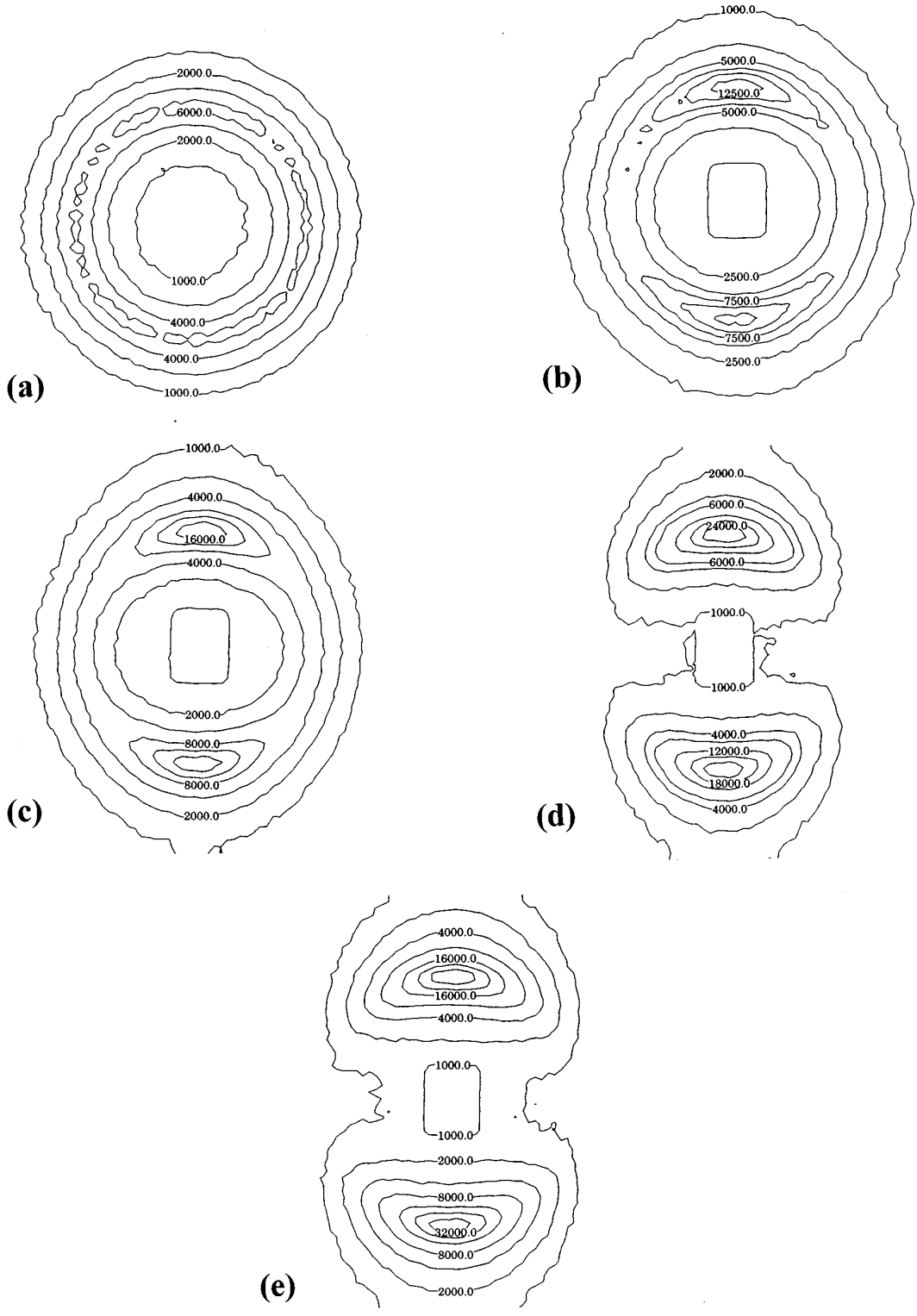

FIG. 8. Contour plot of the measured scattering intensity of the CTAB-D_2O system as observed on the two-dimensional detector. (a)–(d) Plots of measurements made at four different shear rates at 32 °C. (a) Domain I ($\dot{\gamma}=4\ s^{-1}$), (b) and (c) domain II ($\dot{\gamma}=102$ and $250\ s^{-1}$, respectively), (d) domain III ($\dot{\gamma}=1403\ s^{-1}$). (e) CTAB-$D_2O$ nematic solution at $\phi=20\%$ sheared at low $\dot{\gamma}=21.5\ s^{-1}$ and at the same temperature. The full scale in both the $\mathbf{Q}_v$ and $\mathbf{Q}_e$ directions is ± 0.133 Å.

shear stress versus shear rate is obtained using both stress and strain controlled rheometry. In stress controlled experiments, the $\sigma(\dot{\gamma})$ flow curve exhibits two stable branches, one at low-velocity gradients $\dot{\gamma}<\dot{\gamma}_{1c}$, region I, and one at much higher shear rates $\dot{\gamma}>\dot{\gamma}_{2c}$, region III. For the CTAB system at $\phi=18\%$ and $T=32$ °C, one has $\dot{\gamma}_{1c}=6.5\ s^{-1}$ and $\dot{\gamma}_{2c}=420\ s^{-1}$ (Fig. 3). It is noteworthy to recall that all mechanical data displayed in this work are recorded in the stationary state, that is, we have excluded any transient phenomena. As the stress is slowly increased, the response is obtained in

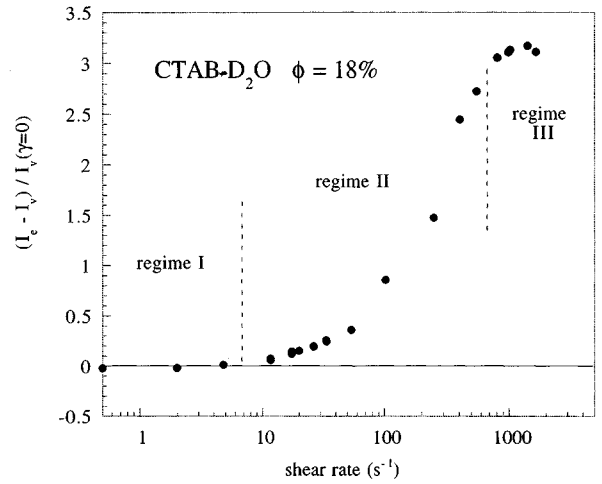

FIG. 9. Shear rate dependence of the anisotropy ratio $[I_e(\dot\gamma) - I_v(\dot\gamma)]/I(\dot\gamma=0)$ as measured from small-angle neutron scattering. The three regimes already identified in rheometry and flow birefringence are shown for comparison. In region III, where saturation is observed, the neutron patterns are identical to those of a nematic phase.

terms of the shear rate, which increases linearily, as expected from a Newtonian regime. At $\dot\gamma_{1c}$ the measured rate jumps suddenly to the much higher strain rate $\dot\gamma_{2c}$ and a true discontinuity occurs. No data points can be taken in the stationary limit in the plateau region II. Such a discontinuity is expected for equilibrium phase transitions in which the extensive parameter, here the shear stress σ is monitored (a liquid-gas transition, for instance). In the log-log representation of $\eta=f(\dot\gamma)$ the shear plateau gives rise to a straight line of slope -1. In the third domain ($\dot\gamma>\dot\gamma_{2c}$) the viscosity is roughly 0.05 Pa s. This value is in agreement with the usual viscosity of the nematic phase [25].

One major finding of the present report is the excellent agreement between the $\sigma(\dot\gamma)$ data as received from strain or stress controlled rheometry. As the inset in Fig. 4 illustrates, not only does the location of the discontinuity in both measurements agree, but so does the height of the plateau ($\sigma = 32$ Pa). In the strain controlled experiments, the sample is forced to flow at a macroscopically imposed and average velocity gradient $\dot\gamma$. Under such conditions, we were able to explore the plateau regime and found out that within the experimental uncertainty, the stress is rigorously constant. Figure 4 and the inset demonstrate in a remarkable way that as long as the system is free to reach the stationary state of flow, the stress plateau is robust and a unique $\sigma(\dot\gamma)$ path is adopted by the system between regions I and III.

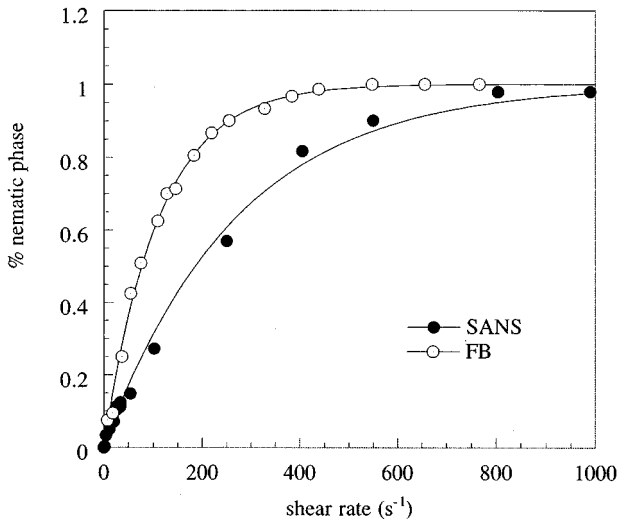

FIG. 10. Variation of the proportion of a nematic phase $P_{\rm nem}(\dot\gamma)$ as derived from small-angle neutron scattering (closed symbols) and from flow birefringence experiments (open symbols). At low shear rates but $\dot\gamma>\dot\gamma_{1c}$, $P_{\rm nem}(\dot\gamma)$ first increases linearly and then saturates on approaching the third regime.

The robustness of the stress plateau was recently reported on another surfactant solution made of cethylpyridinium chloride-sodium salicylate in brine [15]. The observation of a nondegenerated stress plateau in the rheological response of elongated surfactant micelles (no hysteresis) is again a strong indication that a phase transition takes place. However, rheometry alone is clearly unsufficient to assign the physics of the phenomenon. According to the model of Cates and coworkers [6,26], a stress saturation similar to that obtained for other solutions [15] is predicted above a characteristics shear rate $\dot\gamma_{1c}$. The main result of this model is that as shear reaches a threshold value $\dot\gamma_{1c}=2.6/\tau_R$ a mechanical instability of shear banding type occurs within the micellar solutions. This instability is characterized above $\dot\gamma_{1c}$ by a plateau of the shear stress σ at the height $\sigma_c=0.67G_0$.

In this respect, the predictions of Cates and co-workers seem to disagree with the experimental values. In our case, $\dot\gamma_{1c}\tau_R\approx 0.24$ for the CTAB system. The difference probably comes from the origin of the plateau regime. In our previous papers [8,20] we noted that the plateau regime could be interpreted as the coexistence of two concentric different thermodynamical phases present within the shearing cell. These two phases were isotropic and nematic. However, the critical parameters $\dot\gamma_{1c}$ and σ_c in the theory of Cates and co-workers are derived from a criterion of purely mechanical instability of shear banding type. In this case, the theory of Cates and co-workers conceptual framework would not be compatible with the present results.

In order to examine the state of shearing at the stress plateau (region II), flow birefringence and small-angle neutron scattering were undertaken on the same CTAB-D_2O solution, at $\phi=18\%$ and $T=32\,^\circ$C. Note that these measurements were both performed using Couette cells similar to those of the rheological results and correspond to experiments under controlled strain. The photographs obtained in white light and between crossed polarizers of the 1.5-mm gap (cf. Fig. 5) exhibit that, at the onset of the stress plateau, the flow becomes inhomogeneous. Inhomogeneous means here that above the corresponding critical shear rate the velocity field is nonuniform through the gap. Two phases subjected to different shear rates and thus having two different viscosities (since σ remains constant) coexist. When the intensive parameter is monitored to higher values, the proportion of the strongly birefringent phase increases. Similar results have been reported already for protonated solutions of CTAB close to the *I-N* phase boundary [8]. However, here we observe that the third regime depicted by the high-$\dot\gamma$ branch in the flow curve coincides with a gap that is entirely

occupied by the strongly birefringent phase. The shear rate evolution of the bright band is discussed below in reference to the neutron scattering results.

In the experimental configuration of the D11 instrument at the Institut Laue-Langevin, the neutrons (wavelength $\lambda = 6$ Å) provide information on the orientational distribution of the micellar threads on a scale of ~ 100 Å. The intensity received on the detector is the scattering response averaged over a scale that is much larger in real space. It is given typically by the section of the incoming neutron beam (~ 0.5 cm^2). Moreover, due the scattering configuration ($\mathbf{k}_i \| \nabla \mathbf{v}$), this intensity is integrated over the different phases experienced by optical birefringence and encountered on the beam trajectory. With increasing $\dot{\gamma}$ the neutron scattering of CTAB micelles develops an anisotropy in the direction perpendicular to the flow velocity (crescentlike peaks). Keeping the above remarks in mind, the neutron patterns can be interpreted in terms of the superposition of two different contributions [18]: the isotropic ringlike pattern, at best seen in the Newtonian regime (for $\dot{\gamma} < \dot{\gamma}_{1c}$), and the crescentlike peaks typical of the nematic orientational order in the $\mathbf{Q}_e$ direction. The maximum in the scattering function at $Q_{\max} = 0.074$ Å^{-1} indicates a strong correlation ($d \sim 80$ Å) between the centers of masses of the micellar aggregates. The spectrum at $\dot{\gamma} = 13$ s^{-1} is the first for which an anisotropy is detected. Up to $\dot{\gamma}_{1c}$, this anisotropy increases [see Figs. 7(b) and 7(c)] and finally, in region III it dominates entirely the scattering.

In Fig. 9 we have plotted the anisotropy factor defined as $[I_e(\dot{\gamma}) - I_v(\dot{\gamma})]/I(\dot{\gamma}=0)$ at the maximum scattering as a function of the shear rate. Here the maximum intensities are at wave vectors $|\mathbf{Q}_v|$ and $|\mathbf{Q}_e| = 0.074$ Å^{-1}. The rate evolution of the anisotropy factor reveals again the three regions already emphasized. The anisotropy factor is zero below $\dot{\gamma}_{1c}$, increases linearly in the stress plateau region, and then saturates at high $\dot{\gamma}$. In this latter region, the scattering structure factor resembles strongly the one obtained on a nematic phase of the same CTAB-D_2O solution at $\phi = 20\%$ [see Figs. 7(e) and 8(e)]. Therefore, we conclude that the phase showing up at $\dot{\gamma}_{1c}$ in the rheo-optical experiments is a shear-enduced nematic phase. The plateau region corresponds to the biphasic domain of the nonequilibrium phase diagram (under shear).

Assuming finally that the ringlike pattern that persists up to $\dot{\gamma}_{2c}$ can provide an estimate of the remaining isotropic phase (the dark band in the photographs of Fig. 5), we calculate the proportion $P_{\text{nem}}(\dot{\gamma})$ of the nematic phase by the ratio

$$P_{\text{nem}}(\dot{\gamma}) = 1 - \frac{I_v(Q_v = Q_v^{\max}, \dot{\gamma})}{I_v(Q_v = Q_v^{\max}, \dot{\gamma}=0)}. \quad (1)$$

The proportion of the nematic phase determined by Eq. (1) is compared to that derived from the rheo-optical experiments in Fig. 10. For the flow birefringence (FB) data, we simply measure the normalized width of the bright nematic band in terms of the gap size (1.5 mm). $P_{\text{nem}}(\dot{\gamma})$ has similar behavior. The evolution of the proportion of the nematic phase has been shown with two different independent methods. For the shear rate approaching $\dot{\gamma}_{2c}$, the two methods asymptotically give the same results: the shearing solution becomes nematic. However, marked deviations are observed between the SANS and the FB results. For a smaller shear rate, clearly the rheo-optical measurements overestimate the liquid-crystalline proportion with respect to the neutron estimations. Two remarks can be made to explain these deviations. First, it has to be kept in mind that Eq. (1) provides only a rough estimate of one phase with respect to the other. More careful calculations taking into account the azimuthal distribution of neutron counts are needed. Second, a close inspection of the photographs taken in flow birefringence reveals that the bright band showing up close to the inner cylinder wall is subdivided into several small layers [among which some are much less oriented (birefringent)]. The shear-induced menatic band contains thus ''isotropic'' layers that the simple measurement of the bright width ignores systematically.

V. CONCLUSION

The experimental results presented in this work show the effect of a shear rate on a concentrated micellar solution without salt that is isotropic at rest. The system studied, CTAB-D_2O, allows a study at high shear rate, without apparently degradation or expulsion of the sheared sample. This favorable situation allows one to bring to the fore without ambiguity domain III, corresponding to the turnup of the shear stress at high $\dot{\gamma} = \dot{\gamma}_{2c}$. The four techniques used in this work are in good agreement and allow one to understand the evolution of the system towards a complete nematic phase as seen by the SANS under shear experiments and by visual observation between crossed polarizers in the gap of a Couette cell. The critical shear rates $\dot{\gamma}_{1c}$ and $\dot{\gamma}_{2c}$ given from the four techniques, characterizing the beginning and the end of the phase transition, are in good agreement. The flow birefringence technique allows one to show the location of the induced nematic phase in a concentric zone of shear near the moving cylinder. The width of the nematic phase increases with the shear rate up to reach the full gap for $\dot{\gamma} \geqslant \dot{\gamma}_{2c}$. The emergence of the shear plateau corresponds to a real phase transition. The result of it is a band structure formed by different phases (isotropic and nematic). The constant value of the shear stress σ_c when $\dot{\gamma} > \dot{\gamma}_{1c}$ can be explained by the broadening of the nematic band. For the concentrated solution (ϕ close to the concentration corresponding to the static phase I-N transition), the emergence and evolution of a phase transition can easily be understood: the shear rate, as well as the usual thermodynamical parameters (temperature, pressure, etc.), is able to induced it. The full theoretical analysis of the involved mechanism for a salt-free system in which the electrostatic interactions play an important part is still to be done.

[1] S. J. Candau, E. Hirsch, and R. Zana, J. Colloid Interface Sci. **105**, 521 (1985).
[2] S. J. Candau, E. Hirsch, R. Zana, and J. Adam, J. Colloid Interface Sci. **122**, 430 (1988).
[3] G. Porte, J. Appel, and Y. Poggy, J. Phys. Chem. **84**, 3105 (1980).
[4] G. Porte and J. Appel, J. Phys. Chem. **85**, 2511 (1981).
[5] M. E. Cates, J. Phys. Chem. **94**, 371 (1990).
[6] N. A. Spenley, M. E. Cates, and T. C. B. McLeish, Phys. Rev. Lett. **71**, 939 (1993).
[7] H. Hoffmann, S. Hofmann, A. Rauscher, and J. Kalus, Prog. Colloid Polym. Sci. **84**, 24 (1991).
[8] E. Cappelaere, R. Cressely, and J.-P. Decruppe, Colloids Surf. **104**, 353 (1995).
[9] V. Schmitt, F. Schosseler, and F. Lequeux, Europhys. Lett. **30**, 31 (1995).
[10] V. Schmitt and F. Lequeux, J. Phys. (France) II **5**, 193 (1995).
[11] F. Kern, F. Lequeux, R. Zana, and S. J. Candau, Langmuir **10**, 1714 (1994).
[12] S. A. Mackintosh, Safran, and P. A. Pincus, Europhys. Lett. **12**, 697 (1990).
[13] R. Makhloufi, J.-P. Decruppe, A. Aït-ali, and R. Cressely, Europhys. Lett. **32**, 253 (1995).
[14] J.-F. Berret, D. Roux, and G. Porte, J. Phys. (France) II **4**, 126 (1994).
[15] J.-F. Berret, G. Porte, and J.-P. Decruppe, Phys. Rev. E **55**, 1 (1997).
[16] H. Rehage and H. Hoffmann, Mol. Phys. **5**, 933 (1991).
[17] E. Cappelaere and R. Cressely, Colloid Polym. Sci. **275**, (1997).
[18] J.-F. Berret, D. C. Roux, G. Porte, and P. Lindner, Europhys. Lett. **25**, 521 (1994).
[19] V. Schmitt, F. Lequeux, A. Pousse, and D. Roux, Langmuir **10**, 955 (1994).
[20] J.-P. Decruppe, R. Cressely, R. Makhloufi, and E. Cappelaere, Colloid Polym. Sci. **273**, 346 (1995).
[21] P. Linder and Oberthur, Rev. Phys. Appl. **19**, 759 (1984).
[22] V. K. Jindal, J. Kalus, H. Pilsl, H. Hoffmann, and P. Lindner, Journal **94**, 3129 (1990).
[23] J. Kalus, H. Hoffmann, S. H. Chen, and P. Lindner, J. Phys. Chem. **93**, 4267 (1989).
[24] F. Quirion and L. J. Magid, J. Phys. Chem. **90**, 5435 (1986).
[25] P. Panizza, P. Archambault, and D. Roux, J. Phys. (France) II **5**, 303 (1995).
[26] N. A. Spenley, X. F. Yanan, and M. E. Cates, J. Phys. (France) II **6**, 551 (1996).